CHAPTER III
RESULTS

3.1 *Pm*VRP15 mRNA expression in unchallenged- and WSSV-challenged shrimp primary hemocyte cultures

After pre-treatment of primary hemocyte cultures as described in Material and Methods section 2.4, 400 µl of L-15 culture medium was removed from each well and replaced with 400 µl of L-15 culture medium with or without WSSV (~10^4 WSSV viral copies). Then hemocyte cultures were re-incubated at 28 °C for further 24 h. Total RNA was extracted from the hemocytes followed by DNase I, RNase-free treatment, and then single-stranded cDNA was synthesized. RT-PCR was performed using specific primers for *Pm*VRP15, and elongation factor-1 alpha (EF-1α). PCR product was analyzed by 1.5% (w/v) agarose gel electrophoresis, and the differential expression level of *Pm*VRP15 was reported as relative to EF-1α.

3.2 Quantitative analysis of *Pm*VRP15 mRNA expression in response to WSSV infection

In shrimp primary hemocyte cell cultures, *Pm*VRP15 transcript levels were evaluated by Real-time PCR. The results clearly demonstrated that *Pm*VRP15 expression levels in WSSV-infected hemocytes was up-regulated when compared to non-infected hemocytes. *Pm*VRP15 mRNA expression was up-regulated by about 1.1, 2.6, 3.6, 6.7 and 4.1 fold at 6, 12, 24, 48 and 72 h post-infection, respectively (Figure 3.2). These results suggest that hemocyte *Pm*VRP15 transcript is up-regulated in WSSV infection.

3.3 Production of *Pm*VRP15 and GFP dsRNA

The *Pm*VRP15 dsRNA and GFP dsRNA were synthesized using T7 RiboMAX™ Express Large Scale RNA Production System (Promega) following the manufacturer protocol. Double-stranded RNA of *Pm*VRP15 and GFP were analyzed by 1.5% (w/v) agarose gel electrophoresis (Figure 3.3).

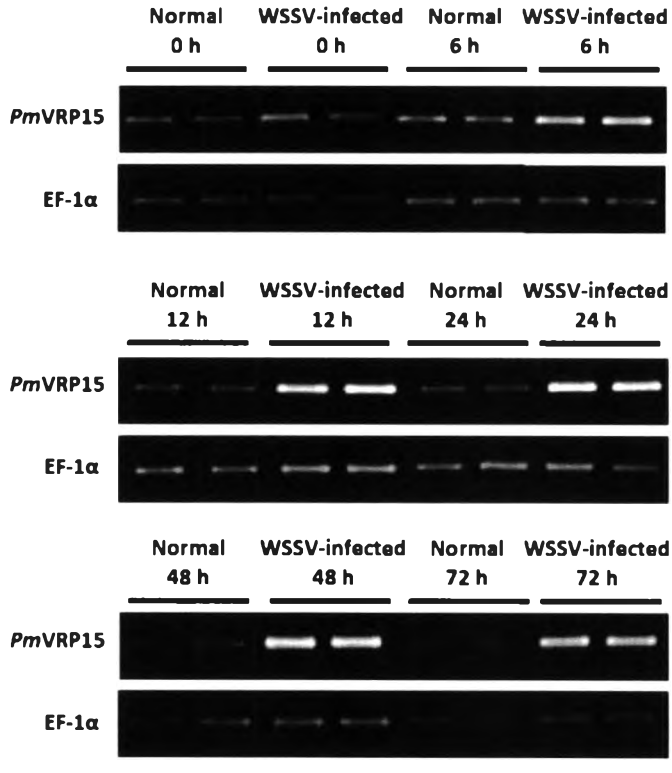

Figure 3.1 *Pm*VRP15 mRNA levels in response to WSSV infection. Relative expression ratios of *Pm*VRP15 transcript levels was determined in WSSV-infected *P. monodon* hemocytes by RT-PCR, compared to control (non-infected) shrimp and standardized against elongation factor-1 alpha (EF-1α) as an internal reference, at 0, 6, 12, 24, 48 and 72 h post-WSSV infection.

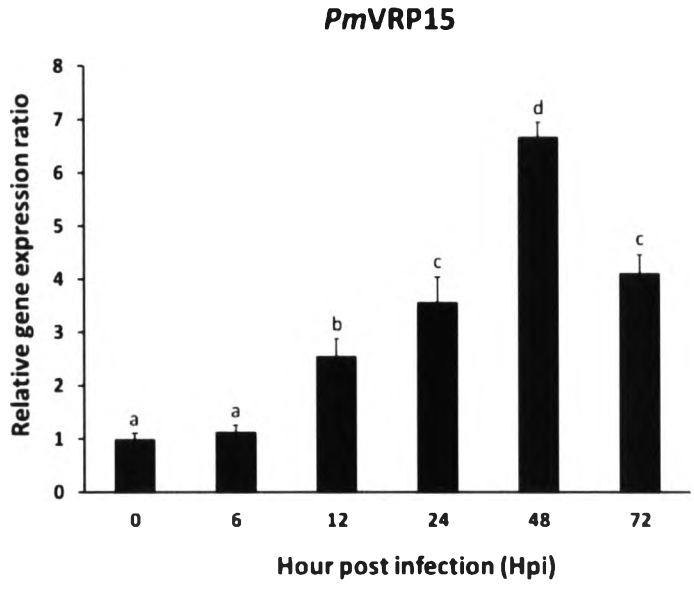

Figure 3.2 Up-regulation of *Pm*VRP15 mRNA in response to WSSV infection. Relative expression ratios of *Pm*VRP15 transcript levels was determined in WSSV-infected *P. monodon* hemocytes by real time RT-PCR, compared to control (non-infected) shrimp and standardized against elongation factor-1 alpha (EF-1 alpha) as the internal reference, at 0, 6, 12, 24, 48 and 72 h post-WSSV infection. The statistical significance of the data was evaluated using one-way ANOVA followed by post hoc test (Duncan's new multiple range test). Data differences were considered significant at $P < 0.01$.

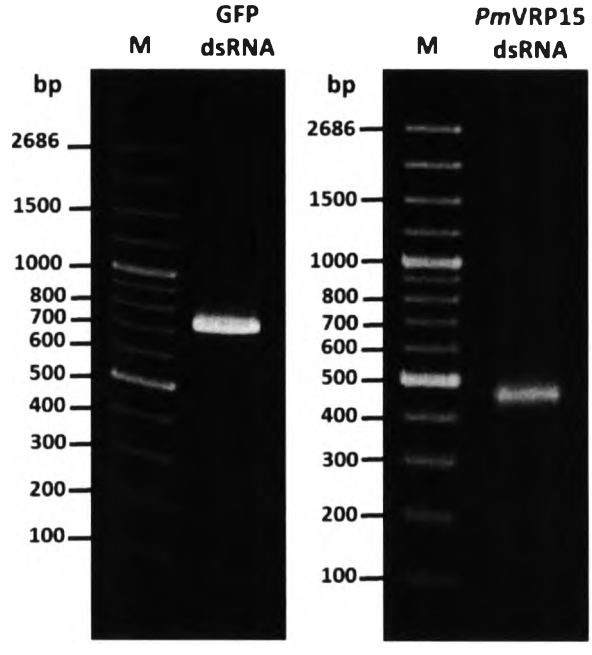

Figure 3.3 Analysis of GFP dsRNA and *Pm*VRP15 dsRNA by 1.5% agarose gel electrophoresis.

3.4 *In vitro* double strand RNA-mediated knockdown of *Pm*VRP15 gene expression resulted in reduction of WSSV propagation by RT-PCR

RNA interference (RNAi) is a powerful strategy to silence the expression of specific genes with dsRNA. RNAi is an important tool for studying gene functions. In this work, dsRNA VRP15 was used to knockdown *Pm*VRP15 transcript to investigate VP28 viral gene expression in primary shrimp hemocyte cultures.

Primary hemocyte cultures were incubated with L-15 or GFP dsRNA (20 μg/well) or *Pm*VRP15 dsRNA (20 μg/well) prior to WSSV injected with L-15 or GFP dsRNA (10 μg/well) or *Pm*VRP15 dsRNA (10 μg/well). For 24 h post-WSSV infection, total RNA was extracted from hemocytes and used for *Pm*VRP15 gene expression analysis by RT-PCR with EF-1α as an internal reference. The result showed that knockdown of *Pm*VRP15 gene in WSSV-infected hemocytes resulted in the reduction of VP28 gene expression (Figure 3.4).

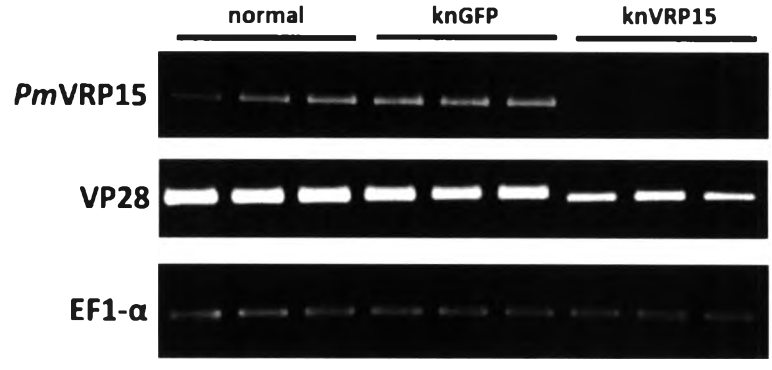

Figure 3.4 Silencing of *Pm*VRP15 expression in WSSV-infected *P. monodon* hemocytes resulted in the reduction of VP28 gene expression. RT-PCR analysis of VP28 and *Pm*VRP15 gene of hemocytes shrimp primary cell culture at 24 hour post WSSV injection.

3.5 *In vitro* double strand RNA-mediated knockdown of *Pm*VRP15 gene expression resulted in reduction of WSSV propagation by Real-time PCR

Viral gene, VP28 transcript levels were evaluated by Real-time PCR. The results demonstrated that VP28 mRNA expression was decreased in shrimp hemocytes after *Pm*VRP15 gene silencing via RNAi. VP28 transcript was reduced by about 4.17 fold (84.29%) at 24 h post WSSV-infection compared to that of normal *P. monodon* hemocytes infected by WSSV (Figure 3.5). This result suggests that *Pm*VRP15 is important for WSSV propagation.

3.6 *Pm*VRP15 is localized in three types of WSSV-infected hemocytes

Effects of *Pm*VRP15 silencing on WSSV infection were observed by confocal laser scanning microscopy (CLSM) using anti-r*Pm*VRP15 antibody with Alexa Fluor® 488 conjugated secondary antibody and anti-VP28 antibody with Alexa Fluor® 568 conjugated secondary antibody. *Pm*VRP15 and VP28 protein were observed as green fluorescence and red fluorescence, respectively. Nuclear DNA of hemocytes was stained with TO-PRO-3 iodine and adjusted to show as blue (Figure 3.6).

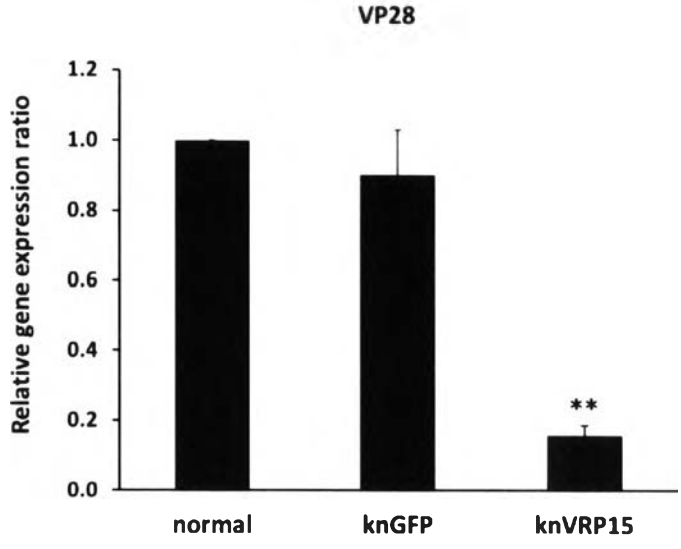

Figure 3.5 Silencing of VRP15 mRNA in response to WSSV propagation. Relative expression ratios of VP28 transcription level was determined in WSSV-infected *P. monodon* hemocytes by real time RT-PCR, compared to control (normal WSSV-infected shrimp hemocytes) and standardized against elongation factor-1 alpha (EF-1 alpha) as an internal reference, at 24 h post-WSSV infection. The data represent the mean (± 1 SD) relative expression of VP28, derived from three independent experiments. Means with an asterisk are significantly different ($P < 0.01$).

Hemocytes collected from *Pm*VRP15-silenced and GFP-silenced of WSSV-infected shrimp were used in this study. The bright field image revealed three types of hemocytes, granular cells (GC) semi-granular cells (SGC) and hyaline cells (HC). Similar to previous study (Vatanavicharn *et al.* 2014), *Pm*VRP15 protein expression was observed in all three types of hemocytes at 48 h post WSSV infection. *Pm*VRP15 protein was located at the edge of nucleus, or possible at the nuclear membrane of the cell. This is in agreement with the fact that *Pm*VRP15 was predicted to contain a transmembrane helix. Hemocytes of kn*Pm*VRP15 showed lower amounts VP28 than those of knGFP cells. This indicated that knockdown of *Pm*VRP15 reduced WSSV propagation.

In *Pm*VRP15-silenced of WSSV-infected hemocytes, the green fluorescent signal of *Pm*VRP15 was still observed, but the intensity of the signal was lower than that observed in GFP-silenced hemocytes. This indicated *Pm*VRP15 was not completely silenced at 48 hpi, the time point at which *Pm*VRP15 was highestly expressed (Figure 3.2).

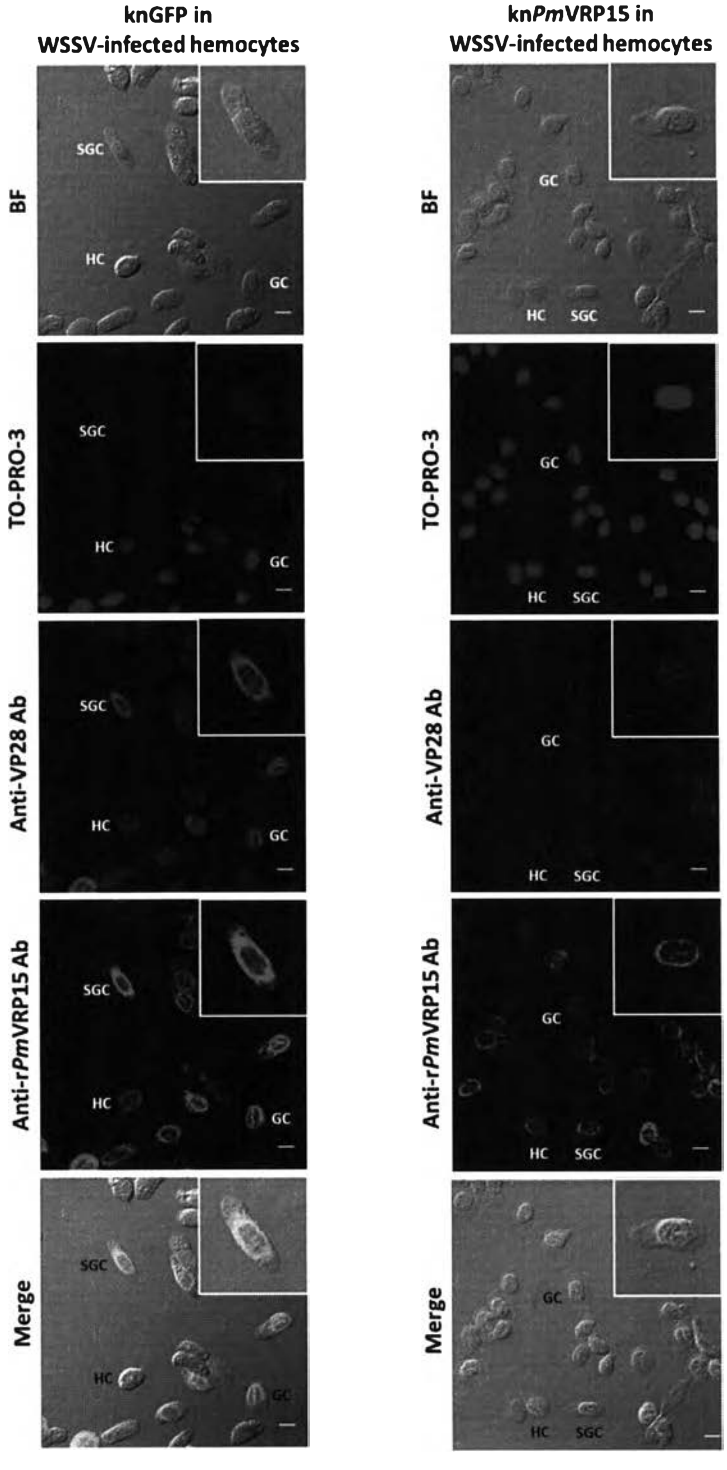

Figure 3.6 Immunofluorescent staining analysis of the *Pm*VRP15 protein content in the *Pm*VRP15 silencing of WSSV-infected hemocytes, in comparison to that of control (GFP silencing of WSSV-infected hemocytes) by confocal laser scanning microscopy. Hemocytes from *Pm*VRP15-silenced and GFP-silenced WSSV-

infected shrimp at 48 hpi were collected (three individual were pooled) and fixed in 4% paraformadehyde. The fixed 1 x 10^6 cells/ml of hemocytes were attached to poly-L-lysine coated slides. The *Pm*VRP15 and VP28 were detected using purified rabbit polyclonal anti-*Pm*VRP15 and purified mouse monoclonal anti-VP28, respectively. The hemocytes were then probed with secondary antibodies conjugated with Alexa Flour 488 (green) for *Pm*VRP15, Alexa Flour 568 (red) for VP28 and TO-PRO-3 iodide (adjusted to blue color) for nuclei staining. The GC, SGC and HC are granular, semigranular and hyaline cells, respectively. BFs are bright field images. The scale bar corresponds to 5 μm. Images are representative of 3 fields of view per sample.

3.7 Confirmation of *Pm*VRP15 knockdown by Western blotting analysis

To study the expression level of *Pm*VRP15, hemocyte lysates were prepared from GFP-silenced and *Pm*VRP15-silenced hemocytes. The expression of *Pm*VRP15 and β-actin of normal and *Pm*VRP15-silenced hemocyte lysate (HLS) were detected by Western blotting. The *Pm*VRP15 protein expression was suppressed in *Pm*VRP15 dsRNA injected shrimp (Figure 3.7). β-actin was found in both normal and *Pm*VRP15-silenced HLS of similar amount, while *Pm*VRP15 was found only in normal hemocytes, but not *Pm*VRP15 silenced HLS (Figure 3.7). The expected size of *Pm*VRP15 and β-actin were about 15 kDa and 43 kDa, respectively. This indicated *Pm*VRP15-silencing resulted in a reduction of *Pm*VRP15 protein.

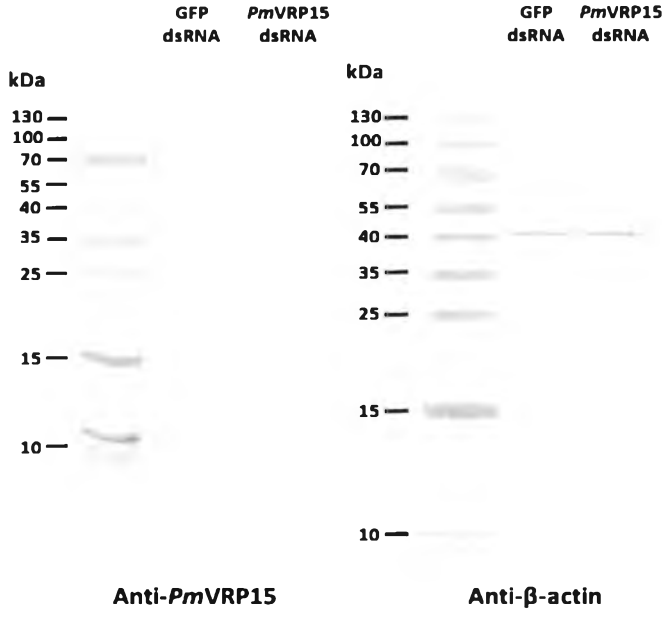

Figure 3.7 RNAi-mediated suppression of *Pm*VRP15 (*Pm*VRP15 dsRNA) resulted in a reduction of protein level compare to GFP dsRNA as a control. The β-actin protein production was used as a control for Western blot analysis.

3.8 Protein localization of *Pm*VRP15 by subcellular protein fractionation in WSSV-infected hemocyte cultures using subcellular fractionation kit

The hemocyte cultures were infected with WSSV and incubated at 27 °C. At 48 h post-WSSV infection, total protein was extracted from hemocytes using Subcellular fractionation kit for cultured cells (Thermo Scientific). Cytoplasmic, membrane, soluble nuclear, chromatin-bound and cytoskeletal fractions were extracted from WSSV-infected hemocyte cultures. The concentration of total protein in each fraction were determined using BCA protein assay and 10 µg of proteins were loaded in each lane. The result was analyzed by SDS-PAGE and Western blotting. *Pm*VRP15 protein was found in soluble nuclear, and chromatin-bound fractions (Figure 3.8). This indicated that *Pm*VRP15 is a nuclear localized protein.

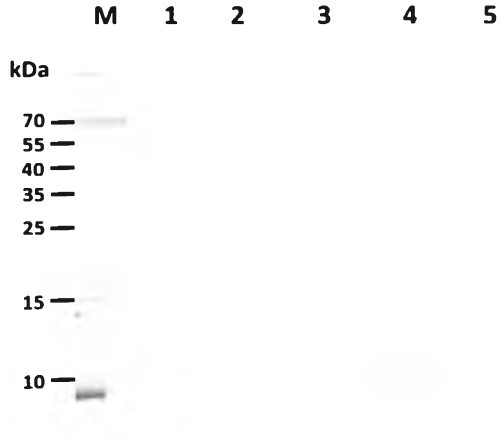

Figure 3.8 Western blotting analysis of the *Pm*VRP15 protein in WSSV-infected hemocytes. Lane M is a protein marker. Lane 1-5 are cytoplasmic, membrane, soluble nuclear, chromatin-bound and cytoskeletal fraction, respectively.

3.9 Quantitation of WSSV copy number in nuclear and cytoplasmic fractions of normal and kn*Pm*VRP15 hemocyte cultures after WSSV infection

The silencing of *Pm*VRP15 in WSSV-infected hemocytes was performed to identify the role of *Pm*VRP15 in nuclear entry or exit of WSSV. Cytoplamic and nuclear fraction were extracted by subcellular fractionation kit. The quantities of

WSSV in each fraction were quantified by Real time RT-PCR with EF-1α as an internal reference. The ratio of DNA virus (WSSV) in nucleus to cytoplasmic fraction of *Pm*VRP15 silenced hemocyte cultures was compared to that of the control (GFP silencing).

In the case that *Pm*VRP15 involved in nuclear entry, the ratio of WSSV DNA in nucleus to cytoplasm of *Pm*VRP15-silenced hemocytes would be lower than that of control. However, if *Pm*VRP15 involved in nuclear exit, the ratio of WSSV DNA in nucleus to cytoplasm would be expected to be higher in *Pm*VRP15-silenced hemocyte cells, compared to that of control.

Table 3.1 shows the ratio of WSSV DNA in nuclear to cytoplasmic fractions of ds*Pm*VRP15 and dsGFP samples. The experiment was carried out in triplicate and EF-1α was used for normalization of WSSV DNA quantification. The result showed that the ratio of DNA virus (WSSV) in nucleus to cytoplasmic fraction of *Pm*VRP15-silenced was lower than that of control (GFP-silenced hemocytes) by 9.28 fold. This suggested that *Pm*VRP15 plays a role in nuclear entry of WSSV.

Table 3.1 The ratio of WSSV copy number of *Pm*VRP15 silencing in nucleus/ cytoplasm compare to control (GFP-silenced hemocytes)

Sample	WSSV in Cytoplasm	WSSV in Nucleus	Average (Nucleus)	Ratio of WSSV in Nucleus/Cytoplasm	Means	Fold
knGFP	3.83E-03	3.92E-02	3.82E-02	9.97E+00	1.11E+01	
	2.95E-03	3.49E-02		1.29E+01		
	3.64E-03	4.04E-02		1.05E+01		
knVRP15	1.60E-02	2.72E-02	1.88E-02	1.17E+00	1.20E+00	**9.28E+00**
	1.47E-02	1.28E-02		1.27E+00		
	1.63E-02	1.62E-02		1.15E+00		

3.9.1 No cross contamination in cytoplasmic and nuclear fractions of WSSV-infected *Pm*VRP15 silenced and control

Cytoplasmic and nuclear fractions of WSSV-infected *Pm*VRP15-silenced and GFP-silenced hemocytes were subjected to Western blotting using Nuclear Pore Complex (NPC) antibody as primary antibody. The result showed that NPC protein was only observed in nuclear fractions of *Pm*VRP15-silenced and GFP-silenced hemocytes. In contrast, NPC protein was not observed in cytoplasmic fractions of *Pm*VRP15- silenced and GFP-silenced hemocytes. This indicated that there was no cross-contamination between cytoplasmic and nuclear fractions (Figure 3.9). Thus, cytoplasmic and nuclear fractions were sent to Charoen Pokphand Foods PCL for determination of the WSSV copy number by Real-time PCR.

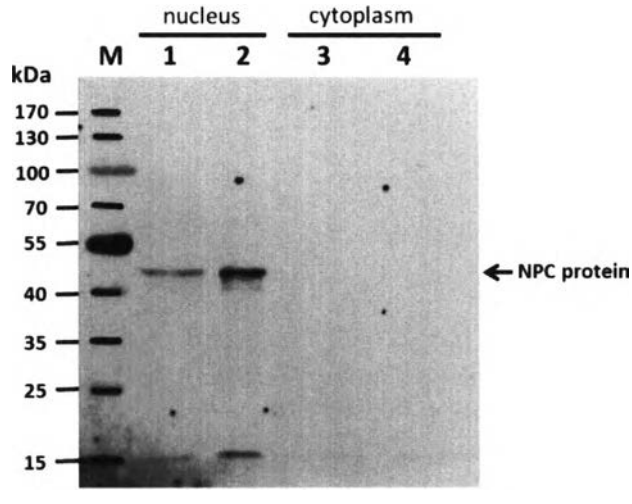

Figure 3.9 Western blot analysis of cytoplasmic and nuclear fractions of WSSV-infected *Pm*VRP15-silenced and GFP-silenced hemocytes using Pierce® Fast Western Blot Kit, SuperSignal® West Femto kit. NPC protein was detected using anti-NPC (Abcam) as primary antibody and Fast Western Mouse Optimized HRP Reagent, Femto as secondary antibody, respectively. X-ray film was developed to observed the signals. Lane 1 is nuclear fractions of WSSV-infected GFP-silenced. Lane 2 is nuclear fractions of WSSV-infected *Pm*VRP15-silenced. Lane 3 is cytoplasmic fractions of WSSV-infected GFP-silenced. Lane 4 is cytoplasmic fractions of WSSV-infected GFP-silenced.

3.10 Expression of r*Pm*VRP15 protein in *Saccharomyces cerevisiae*

3.10.1 Amplification of *Pm*VRP15 gene

*Pm*VRP15 gene was amplified with *Pm*VRP15-F and *Pm*VRP15-R primers (Table 2.4) that include 5' overhangs complementing the upstream and downstream sequences to either side of the *Sma* I site in pDDGFP-2 vector. The PCR products of *Pm*VRP15 gene were analyzed by 1.5% agarose gel electrophoresis (Figure 3.12). The size of *Pm*VRP15 gene was about 414 bp.

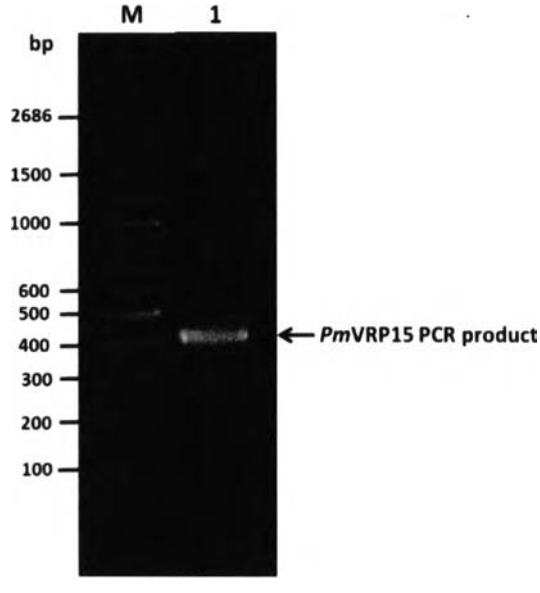

Figure 3.10 Amplification of *Pm*VRP15 gene (lane1) with specific primers (Table 2.4) that include 5' overhangs complementing the upstream and downstream sequences to either side of the *Sma* I site in pDDGFP-2 vector. Lane M is 100 bp DNA ladder. Lane 1 is PCR product of *Pm*VRP15.

3.10.2 Digestion of pDDGFP-2 vector with *Sma* I

The pDDGFP-2 vector was digested by *Sma* I. The reaction of 20 µl total volume contained 1 unit of *Sma* I, 10X buffer 4 and 10 µl of pDDGFP-2 vector (50 ng/µl). The reaction were incubated at 37 °C overnight, followed by heat inactivated at 65 °C for 20 min. The *Sma* I-linearized pDDGFP-2 was analyzed by comparing with non-digested pDDGFP-2 vector by 1% agarose gel electrophoresis and visualized by gel documentation system (SynGene) (Figure 3.13). The result showed that pDDGFP-2

vector was digested with *Sma* I (lane 2) as DNA bands was shifted in agarose gels compared to non-digested pDDGFP-2 vector (lane 1).

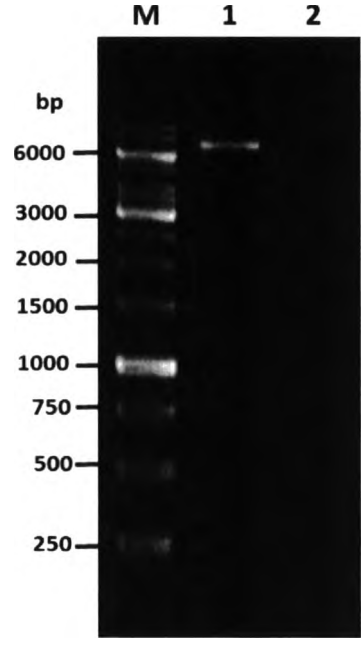

Figure 3.11 Analysis of *Sma* I-linearized pDDGFP-2 vector (lane 2) compare with non-digested pDDGFP-2 vector (lane 1). Lane M is GeneRuler™ 1 kb DNA ladder.

3.10.3 Production of recombinant *Pm*VRP15 (r*Pm*VRP15) in *S. cerevisiae* expression system

Crude r*Pm*VRP15 in *S. cerevisiae* (FGY217) was analyzed by 15% SDS-PAGE compared to non-galactose induced r*Pm*VRP15 (Figure 3.12). The result showed that r*Pm*VRP15 protein did not overexpress in *S.cerevisiae* (FGY217). In Figure 3.13, soluble and inclusion bodies protein of r*Pm*VRP15 were analyzed compared with control at 0 h and 22 h post-galactose induction by 15% SDS-PAGE. No major protein band was observed in soluble and inclusion bodies fractions of induction samples.

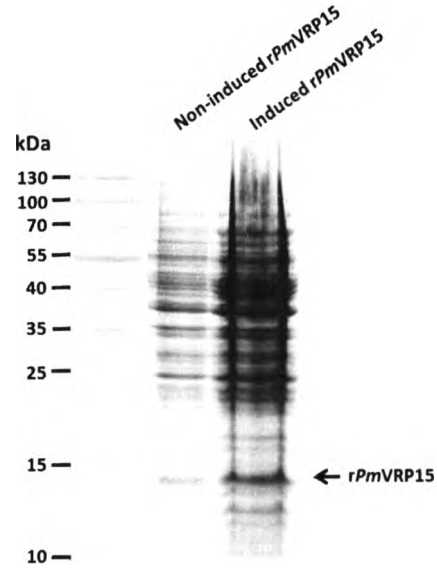

Figure 3.12 Protein expression of crude r*Pm*VRP15 in *S. cerevisiae* (FGY217) post-galactose induction at 22 h compared to non-galactose induced r*Pm*VRP15.

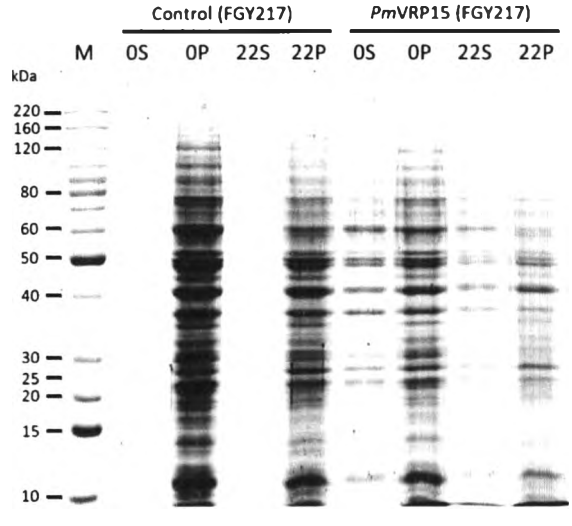

Figure 3.13 Protein expression of r*Pm*VRP15 in *S.cerevisiae* (FGY217) compare with control (FGY217). (0S; soluble protein at 0 h post-galactose induction, 0P; pellet or inclusion bodies protein at 0 h post-galactose induction, 22S; soluble protein at 22 h post-galactose induction, 22P; pellet or inclusion bodies protein at 22 h post-galactose induction).

3.11 Cloning and expression of full-length and truncated r*Pm*VRP15 protein in *E. coli* expression system

3.11.1 Amplification of full-length and truncated r*Pm*VRP15

Full-length and truncated r*Pm*VRP15 was amplified by PCR from cDNA library using a specific primer (Table 2.5). PCR products size of full-length, N-terminal and C-terminal truncated *Pm*VRP15 were about 414 bp, 112 bp and 229 bp, respectively.

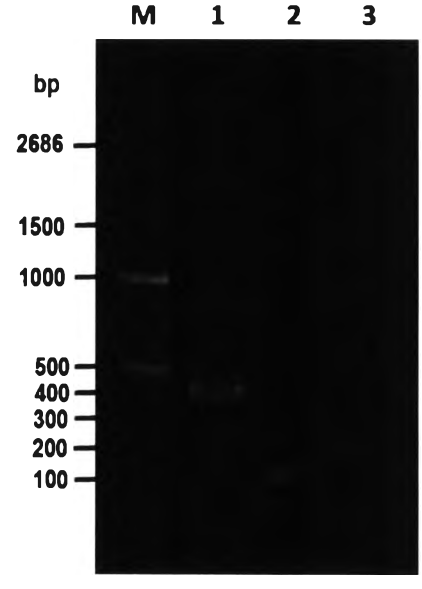

Figure 3.14 PCR products of full-length (414 bp), N-terminal truncated (112 bp) and C-terminal truncated (229 bp) of *Pm*VRP15. Lane 1 is full-length of *Pm*VRP15 gene. Lane 2 is N-terminal truncated of *Pm*VRP15 gene. Lane 3 is C-terminal truncated of *Pm*VRP15 gene.

3.11.2 Expression of full-length and truncated r*Pm*VRP15 in *E. coli* system

Full-length *Pm*VRP15-recombinant pGEX4T-3 was expressed in *E. coli* C41 (DE3) and C43 (DE3) at highest level at 1 hour after induction with IPTG (final concentration 1 mM IPTG). The amount of full-length *Pm*VRP15-GST fusion protein was decreased at 3 and 5 hour (Figure 3.15). This may due to either *Pm*VRP15 was toxic or unstable. It was also shown that full-length *Pm*VRP15-GST fusion protein was expressed mostly in inclusion bodies and slightly in soluble form. Similarly, N-terminal truncated *Pm*VRP15 was expressed in *E. coli* C41 (DE3) and C43 (DE3) in

inclusion bodies (Figure 3.16). This indicated that removal of predicted transmembrane helix of *Pm*VRP15 did not increase protein solubility. C-terminal truncated *Pm*VRP15 was expressed in *E. coli* BL21-CodonPlus® (DE3) at 37°C in inclusion bodies. The protein was expressed at the same level at 1, 3 and 5 hour after IPTG induction (Figure 3.17A). This showed that C-terminal truncated *Pm*VRP15 was stably expressed in *E. coli* BL21-CodonPlus® (DE3). C-terminal truncated *Pm*VRP15 was then expressed in *E. coli* BL21-CodonPlus® (DE3) at 16°C. It was shown that C-terminal truncated *Pm*VRP15-GST fusion protein was expressed mostly in inclusion bodies and slightly in soluble form (Figure 3.17B). Accordingly, protein expression at lower temperature did not help increase protein solubility.

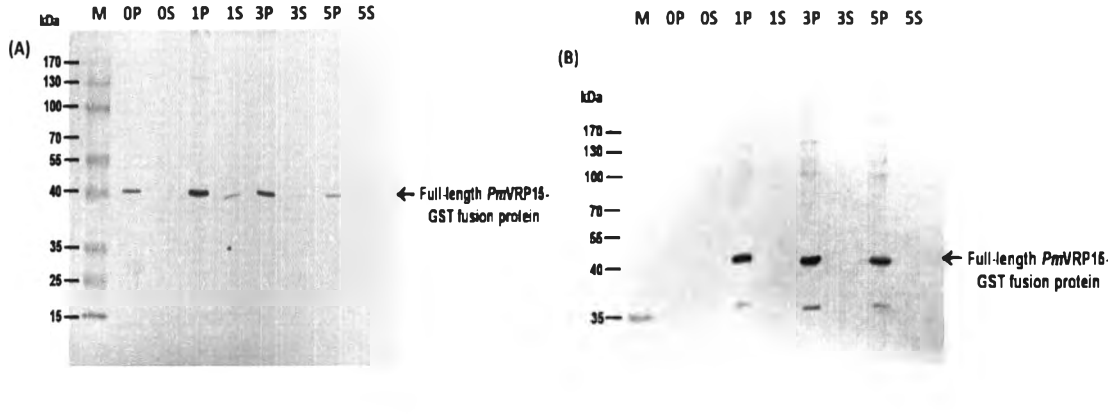

Figure 3.15 Western blotting analysis of full-length *Pm*VRP15-recombinant pGEX4T-3. The recombinant protein was expressed in *E. coli* C41 (DE3) (A) and *E. coli* C43 (DE3) (B) at 0 h, 1 h, 3 h and 5 h after induction by IPTG at 37°C (S; soluble fraction, P; pellet or inclusion bodies protein fraction). An arrow indicates full-length *Pm*VRP15-GST fusion protein.

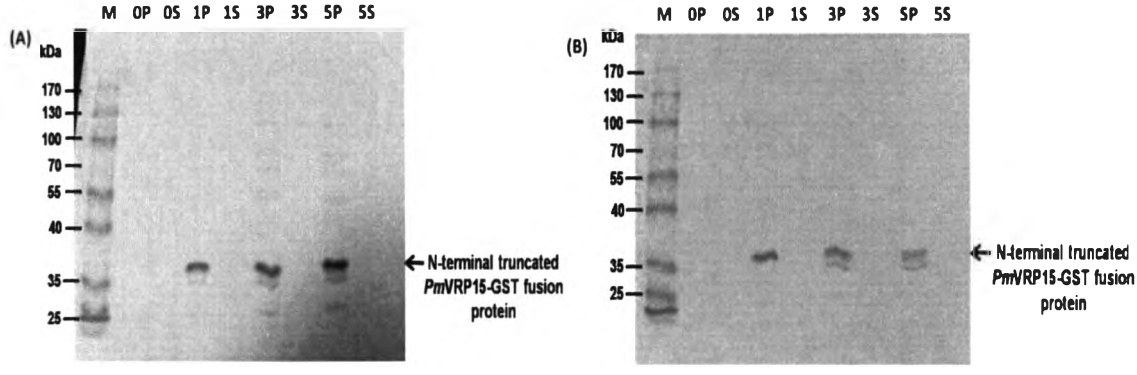

Figure 3.16 Western blotting analysis of N-terminal truncated *Pm*VRP15-recombinant pGEX4T-3. The recombinant protein was expressed in *E. coli* C41 (DE3) (A) and *E. coli* C43 (DE3) (B) at 0 h, 1 h , 3 h and 5 h after induction by IPTG at 37°C (S; soluble fraction, P; pellet or inclusion bodies protein fraction). An arrow indicates N-terminal truncated *Pm*VRP15-GST fusion protein.

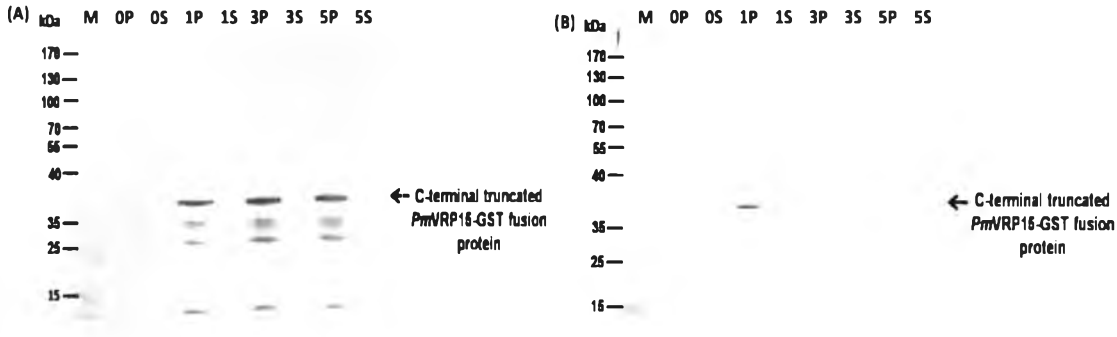

Figure 3.17 Western blotting analysis of C-terminal truncated *Pm*VRP15-recombinant pGEX4T-3. The recombinant protein was expressed in *E. coli* BL21-CodonPlus® (DE3) at 37 °C (A) and 16 °C (B) at 0 h, 1 h, 3 h and 5 h after induction by IPTG (S; soluble fraction, P; pellet or inclusion bodies protein fraction). An arrow indicates C-terminal truncated *Pm*VRP15-GST fusion protein.

3.12 Expression and purification of r*Pm*VRP15 in *E. coli* expression system

3.12.1 Expression of r*Pm*VRP15 in *E. coli* C43 (DE3)

Full-length r*Pm*VRP15 was produced in the *E. coli* C43 (DE3) induced by adding IPTG to final concentration of 1 mM and then incubated for 0, 1, 2, 3, 4, 5 and 6 h at 37 °C. Expression of r*Pm*VRP15 was analyzed by SDS-PAGE. The result showed that the r*Pm*VRP15 was expressed at 1-3 h post-IPTG induction and expressed in the highest level at 2 h post-IPTG induction (Figure 3.18). Interestingly, no r*Pm*VRP15 band was observed on Western blot membrane after 3 h post-IPTG induction (Figure 3.18B).

This indicated that r*Pm*VRP15 was a toxic protein or it was unstable, so no full-length *Pm*VRP15 protein band was detected after 3 h IPTG-induction. From Western blotting analysis, most of r*Pm*VRP15 was found in inclusion bodies and only slightly amount of protein was found (Figure 3.19). This may due to the fact that *Pm*VRP15 contained a transmembrane helical domain.

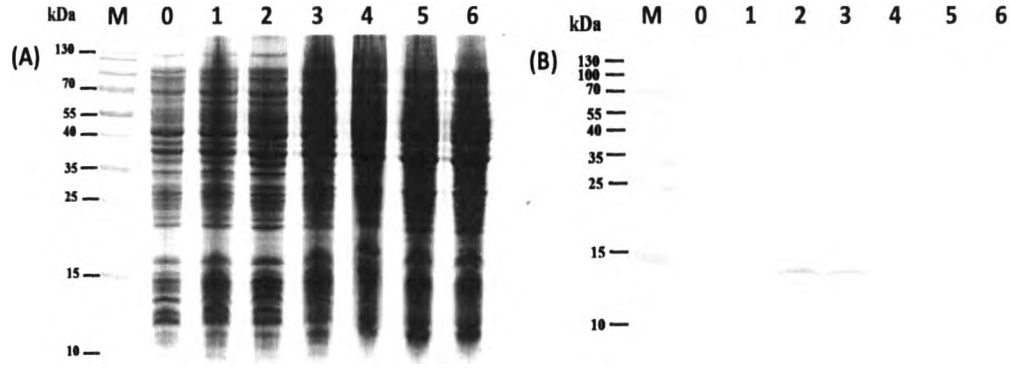

Figure 3.18 Expression of r*Pm*VRP15 in *E. coli* C43 (DE3). The r*Pm*VRP15 was expressed in *E. coli* C43 (DE3) and induced with 1 mM IPTG for 0, 1, 2, 3, 4, 5 and 6 hour. Expression of r*Pm*VRP15 was analyzed by 15% SDS-PAGE followed by coomassie brilliant blue staining (A) and Western blotting (B). Lane M is the protein marker.

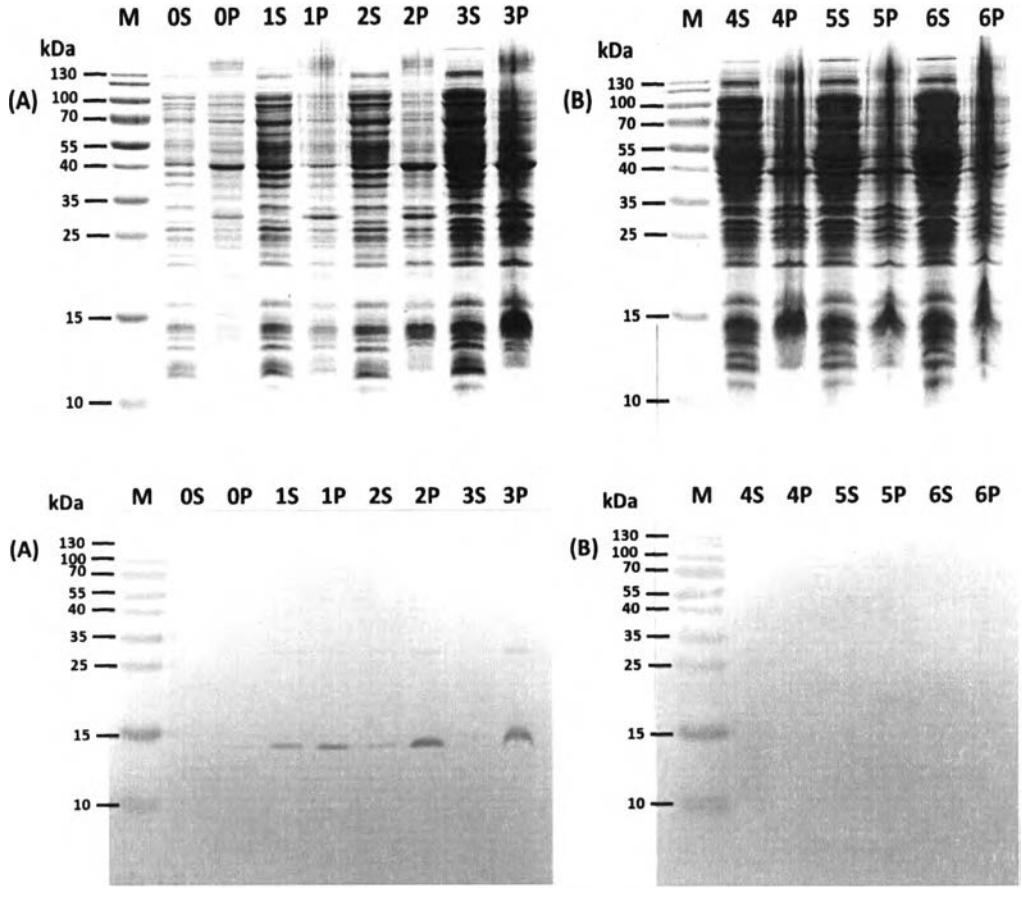

Figure 3.19 Coomassie brilliant blue staining (upper panel) and Western blot analysis (lower panel) of r*Pm*VRP15 in *E. coli* C43 (DE3). (S; soluble fraction, P; pellet or inclusion bodies protein fraction).

3.12.2 Purification of the r*Pm*VRP15 by Nikel-nitrilotriacetic acid (Ni-NTA) Sepharose™ 6 Fast Flow (GE Healthcare)

The r*Pm*VRP15 protein was solubilized in solubilization buffer (50 mM Tris-HCl, pH 7.0, 20 mM Imidazole, 300 mM NaCl, 20% glycerol and 1% DM) at 4 °C overnight. Protein was purified using the affinity chromatography by Ni-NTA Sepharose™ 6 Fast Flow (GE Healthcare). The purity of r*Pm*VRP15 was analyzed by 15% SDS-PAGE (Figure 3.20). Unbound proteins was shown in lane F (Flow-through) and lane W (washed fraction). The eluted proteins were shown in lane 1-3. Very large band of protein of approximately 15 kDa was found in eluted fractions of 300 mM

Imidazole. This protein band is supported to be r*Pm*VRP15. At this point, it seems like *Pm*VRP15 was partially purified by Ni-NTA column.

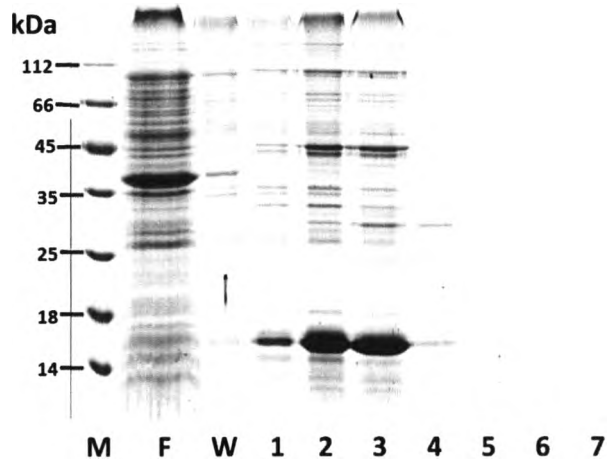

Figure 3.20 15% SDS-PAGE analysis of purified r*Pm*VRP15 by Ni-NTA Sepharose™ 6 Fast Flow. Lane M is the protein marker, lane F is flow-through, lane W is washed fraction, lane 1-4 is eluted fraction with 300 mM imidazole and lane 5-7 is eluted fraction with 500 mM imidazole.

3.12.3 Purification of the r*Pm*VRP15 by HiTrap DEAE Fast Flow (GE Healthcare)

The eluted protein fractions from Ni-NTA column was pooled and dialyzed against dilution buffer (10 mM Tris-HCl, pH 7.0, 2.5% glycerol and 0.07% DM). r*Pm*VRP15 protein was further purified by weak anion exchanger chromatography, a HiTrap DEAE Fast Flow column. Flow-through, washed and eluted protein fractions of HiTrap DEAE FF column were analyzed by 15% SDS-PAGE (Figure 3.21). A large protein band of 15 kDa was found in eluted fractions (20 mM Tris-HCl, pH 7.0, 150 mM NaCl, 5% glycerol and 0.1% DM). In lane 1, *Pm*VRP15 was purified to a single protein band. Eluted fractioned were then pooled and subjected to Western blot analysis.

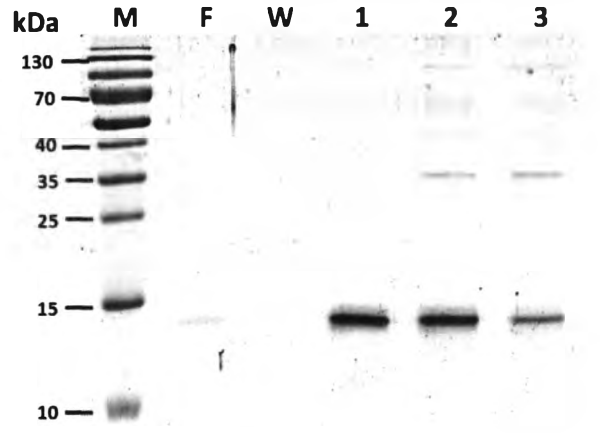

Figure 3.21 15% SDS-PAGE analysis of purified r*Pm*VRP15 by HiTrap DEAE Fast Flow. Lane M is the protein marker, lane F is flow-through, lane W is washed fraction, lane 1-3 is eluted fraction with elution buffer (20 mM Tris-HCl, pH 7.0, 150 mM NaCl, 5% glycerol and 0.1% DM).

3.12.4 Confirmation of purified r*Pm*VRP15 by Western blot analysis

Purified r*Pm*VRP15 protein was confirmed by Western blotting analysis. Membrane was incubated with a 1:3,000 dilution of mouse anti-His antibody at 37 °C for 3 h. After washing with PBST, membrane was incubated in a secondary antibody solution, the alkaline phosphatase-conjugated rabbit anti-mouse IgG, 1:10,000 dilution at RT for 1 hour and detected in darkness with 10 ml of detection buffer (100 mM Tris-HCl, 100 mM NaCl and 50 mM MgCl2, pH 9.5) containing 44 µL of NBT and 33 µL of BCIP as substrate. The protein band of 15 kDa was identified as r*Pm*VRP15 using anti-His antibody (Figure 3.22).

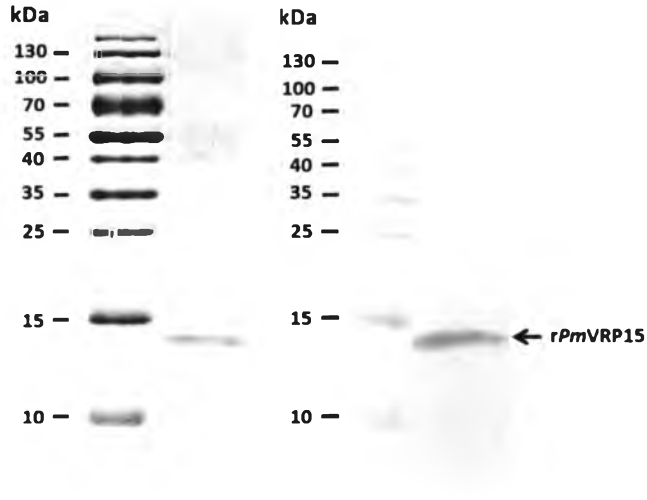

Figure 3.22 15% SDS-PAGE followed by coomassie brilliant blue staining (A) and Western blotting (B) analysis of purified r*Pm*VRP15

3.13 Determination of r*Pm*VRP15 using MALDI-TOF Mass spectrometry (MALDI-TOF MS)

To determine the molecular weights of r*Pm*VRP15, purified r*Pm*VRP15 was sent to Mahidol University for MALDI-TOF MS analysis. The result showed that molecular mass of r*Pm*VRP15 was 15,899.9 Da (Figure 3.23).

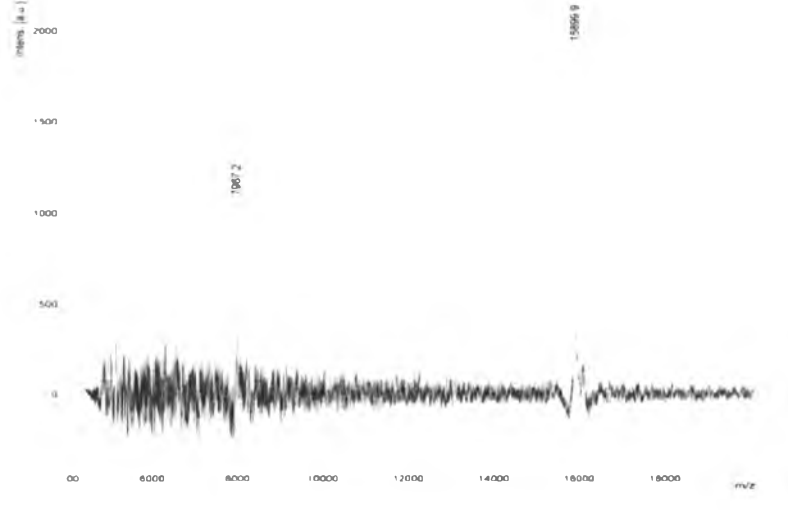

Figure 3.23 MALDI-TOF mass spectrometry analysis of r*Pm*VRP15. Molecular mass of r*Pm*VRP15 was 15,899.9 Da.

3.14 Determination of secondary structure of r*Pm*VRP15 using Circular Dichroism (CD) spectroscopy

To determine the secondary structure of r*Pm*VRP15, Circular dichroism (CD) spectroscopy was used. CD spectra of r*Pm*VRP15 revealed that the major secondary structure type of r*Pm*VRP15 was alpha-helix (Figure 3.24B), in comparison to standard protein which known secondary structure (Figure 3.24A).

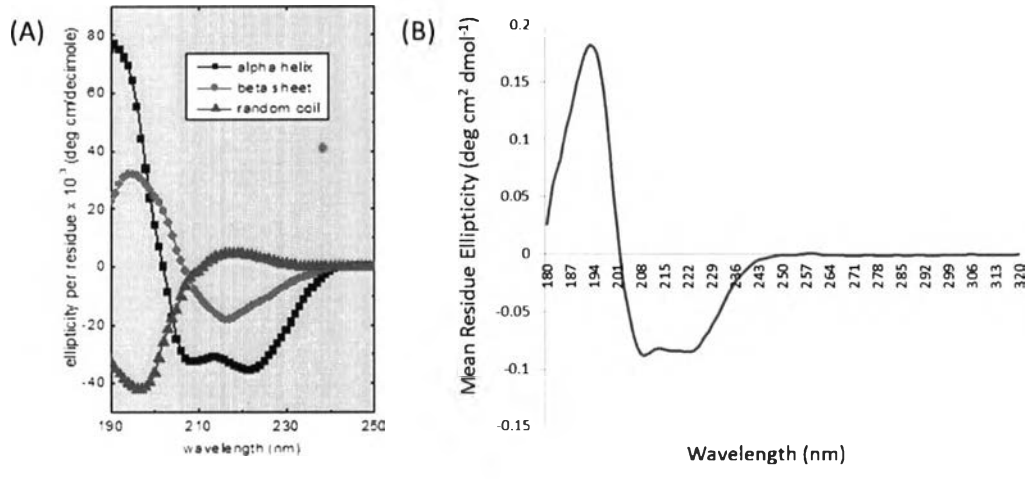

Figure 3.24 CD spectropolarimeter showed the characteristic spectra of different types of secondary structure (A) and CD spectra of r*Pm*VRP15 (B). The major seconadary structure type of r*Pm*VRP15 was alpha-helix.

The amount of regular secondary structures (α-helix and β-strand) were estimated by analysis of the CD spectra using K2D3 deconvolution software (Louis-Jeune *et al.* 2011). The result showed that the predicted secondary structure percentages of r*Pm*VRP15 was 48.45% α-helix and 13.57% β-strand (Figure 3.25).

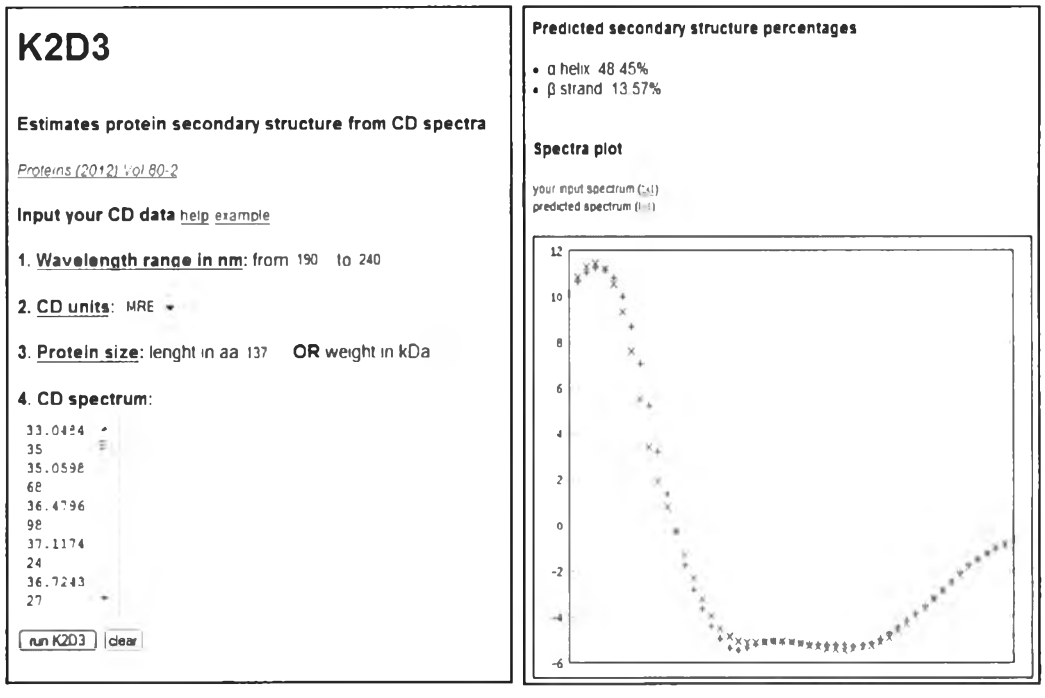

Figure 3.25 Analysis of predicted secondary structure percentages of r*Pm*VRP15 using K2D3 deconvolution software.

3.15 Pre-crystallization test by PCT™ (Hampton Research)

The PCT ™ (Pre-Crystallization Test) was used to determine the appropriate protein concentration for crystallization screening (Aleksandra and Christopher., 2005). The appropriate precipitate was observed in the drop using a light microscope with magnification between 20X and 100X and compare the results to those in Figures 2.26.

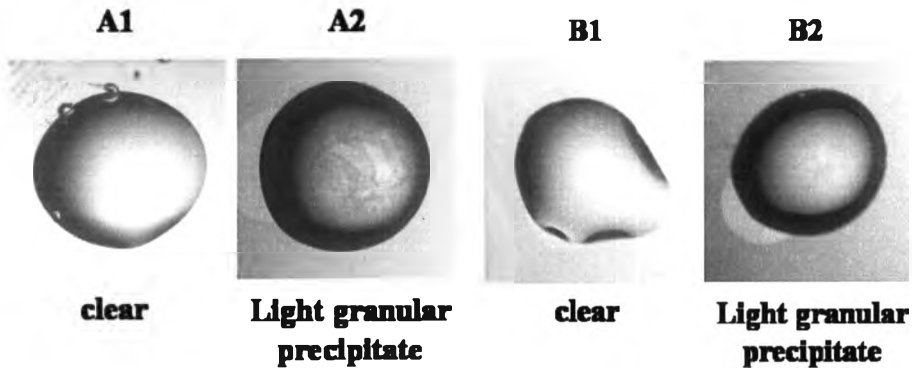

Figure 3.26 PCT Reagent A1/A2 and B1/B2 results of r*Pm*VRP15 protein using a light microscope.

The r*Pm*VRP15 of 2 mg/ml was mixed with A1/A2 and B1/B2 reagents. A clear drop was observed with A1 and B1 solutions, while a light granular precipitate drop was found with A2 and B2 solutions. This indicated that 2 mg/ml of r*Pm*VRP15 was suitable for crystallization screening.

3.16 Protein crystallization

Purified r*Pm*VRP15 was mixed with Index™, MembFac™ and CrystalScreen 2™ reservoir solutions (Hampton Research) in 96-well plate by the sitting drop vapor diffusion method. Crystals of r*Pm*VRP15 appear in 6 conditions (Figure 3.27).

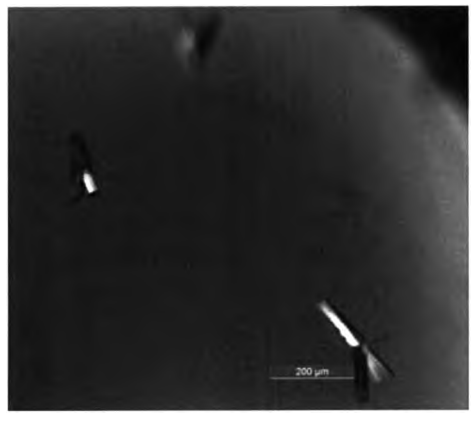

Index™ D12

- 0.2 M Calcium chloride dihydrate
- 0.1 M BIS-TRIS pH 5.5
- 45% v/v (+/-)-2-Methyl-2,4-pentanediol

Index™ E1

- 0.2 M Calcium chloride dihydrate
- 0.2 M BIS-TRIS pH 6.5
- 45% v/v (+/-)-2-Methyl-2,4-pentanediol

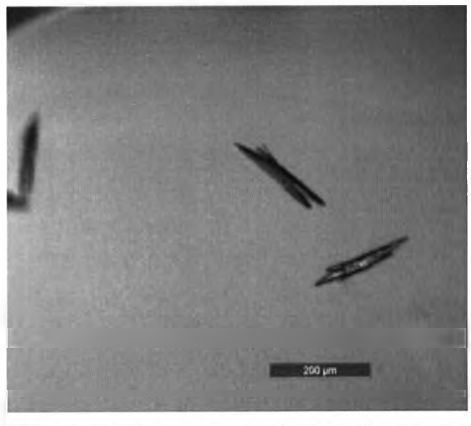

Index™ E6

- 0.05 M Calcium chloride dihydrate
- 0.1 M BIS-TRIS pH 6.5
- 30% v/v Polyethylene glycol monomethyl ether 550

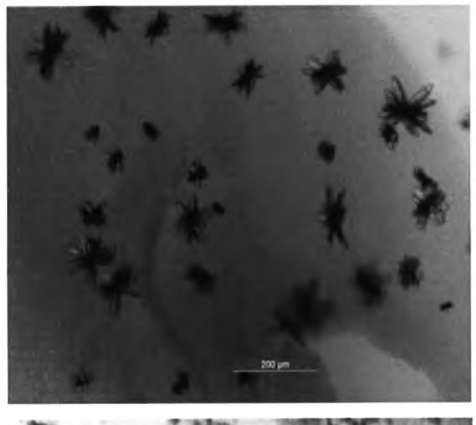

Index™ H9

- 0.05 M Zinc acetate dihydrate
- 20% w/v Polyethylene glycol 3,350

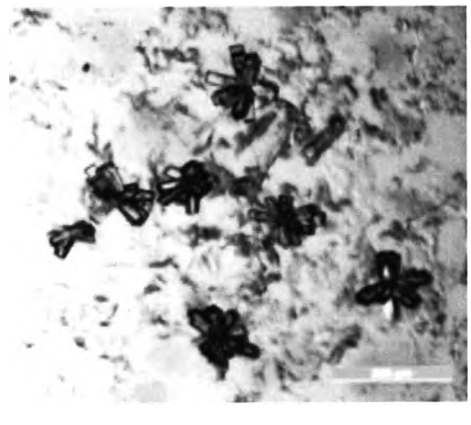

MembFac™ A2

- 0.1 M Zinc acetate dihydrate
- 0.1 M Sodium acetate trihydrate pH 4.6
- 12% w/v Polyethylene glycol 4,000

Crystal screen 2™ H3

- 0.2 M Magnesium chloride
- 0.1 M TRIS-HCl pH 8.5
- 2.6 M 1,6-Hexane diol

Figure 3.27 Crystals appear in different conditions in 96-well plate. Drops of protein and reservoir solution were set up at the ratio of 1:1 and incubated at 18 °C. Crystallization plates were observed after 2 weeks under Leica® microscope.

Crystals were then reproduced in a 24-well plate and subjected to X-ray diffraction test. So far crystals from Index™ D12, H9 and MembFac™ A2 conditions were test at beamline BL13B1 at the National Synchrotron Radiation Research Center (NSRRC), Taiwan. Crystals from Index™ H9 condition gave strong spots in the diffraction (Figure 3.28), indicating that the crystals are salt. Meanwhile, crystals from MembFac™ A2 condition did not diffract (Figure 3.29). This may be caused by several factors, for example, disorder crystals and inappropriate cryoprotectants. In Figure 3.30, a diffraction image of a crystal from Index™ D12 condition showed close spots at low resolution (~9 Å), suggesting the presence of proteins.

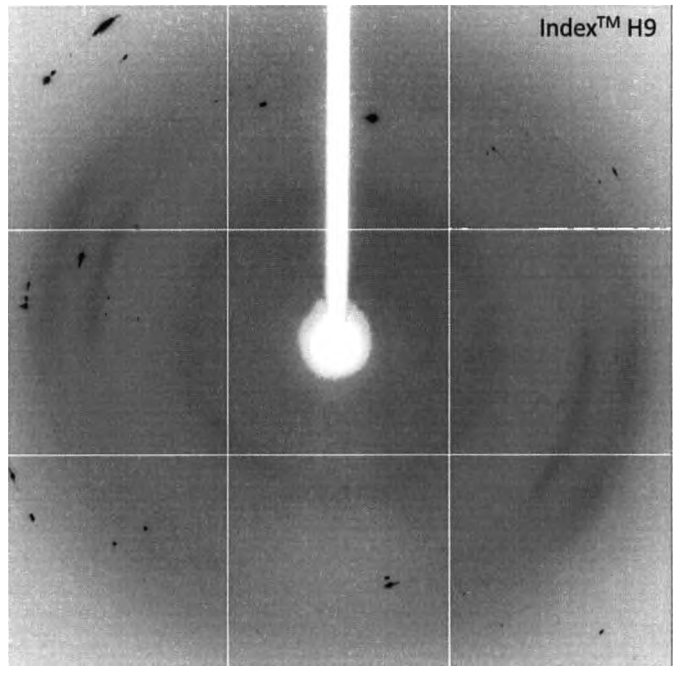

Figure 3.28 A diffraction image of Index™ H9 crystal, tested on beamline BL13B1 of NSRRC using an ADSC Quantum 315 CCD detector. The X-ray wavelength was 1 Å and the image was taken using a 30 sec exposure time and 1.0 Å oscillation range.

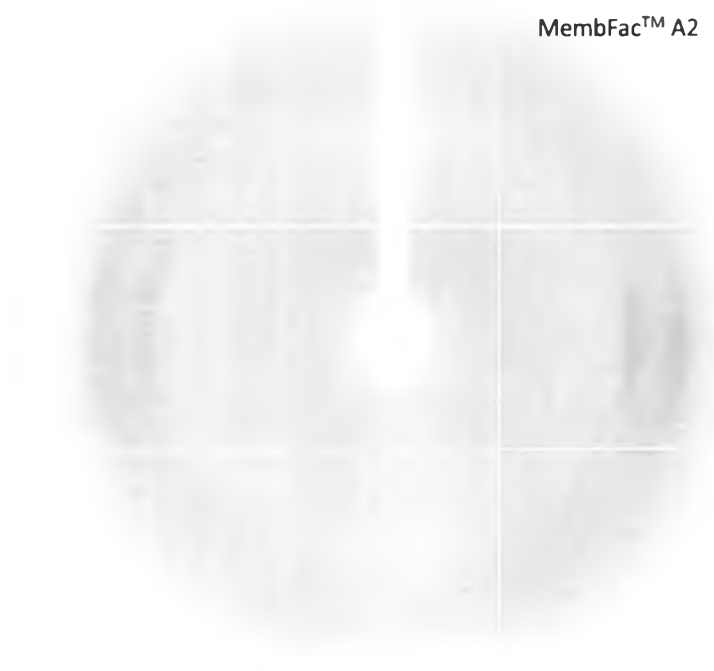

Figure 3.29 A diffraction image of MembFac™ A2 crystal, tested on beamline BL13B1 of NSRRC using an ADSC Quantum 315 CCD detector. The X-ray wavelength was 1 Å and the image was taken using a 30 sec exposure time and 1.0 Å oscillation range.

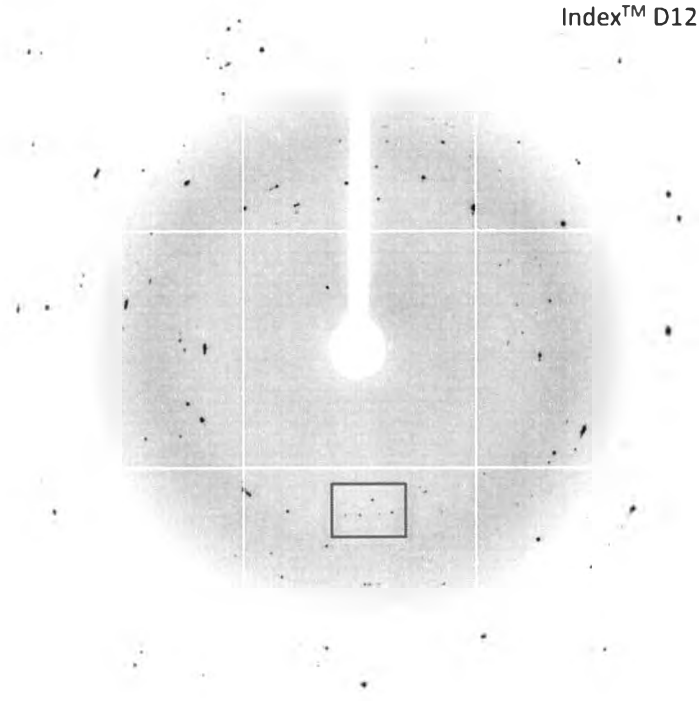

Figure 3.30 A diffraction image of Index™ D12 crystal, tested on beamline BL13B1 of NSRRC using an ADSC Quantum 315 CCD detector. The X-ray wavelength was 1 Å and the image was taken using a 30 sec exposure time and 1.0 Å oscillation range. Ambiguous protein spots are in red box.